



# LUND UNIVERSITY

## High-resolution absorption measurements by use of two-tone frequency-modulation spectroscopy with diode lasers

Avetisov, V. G; Kauranen, P

*Published in:*  
Applied Optics

*DOI:*  
[10.1364/AO.36.004043](https://doi.org/10.1364/AO.36.004043)

1997

[Link to publication](#)

*Citation for published version (APA):*  
Avetisov, V. G., & Kauranen, P. (1997). High-resolution absorption measurements by use of two-tone frequency-modulation spectroscopy with diode lasers. *Applied Optics*, 36(18), 4043-4054.  
<https://doi.org/10.1364/AO.36.004043>

*Total number of authors:*  
2

### General rights

Unless other specific re-use rights are stated the following general rights apply:  
Copyright and moral rights for the publications made accessible in the public portal are retained by the authors and/or other copyright owners and it is a condition of accessing publications that users recognise and abide by the legal requirements associated with these rights.

- Users may download and print one copy of any publication from the public portal for the purpose of private study or research.
- You may not further distribute the material or use it for any profit-making activity or commercial gain
- You may freely distribute the URL identifying the publication in the public portal

Read more about Creative commons licenses: <https://creativecommons.org/licenses/>

### Take down policy

If you believe that this document breaches copyright please contact us providing details, and we will remove access to the work immediately and investigate your claim.

LUND UNIVERSITY

PO Box 117  
221 00 Lund  
+46 46-222 00 00

# High-resolution absorption measurements by use of two-tone frequency-modulation spectroscopy with diode lasers

Viacheslav G. Avetisov and Peter Kauranen

The capability of two-tone frequency-modulation spectroscopy (TTFMS) in deriving spectral line-shape information was investigated. Two oxygen A-band transitions at 760 nm were selected, and the Voigt profile and two different collisionally narrowed line profiles were employed in their analysis. By means of a least-squares fitting procedure, we obtained accurate information regarding transition strengths and pressure-induced broadening, shift, and narrowing coefficients. Both TTFMS and direct absorption line shapes were modeled with deviations as small as 0.3% over a wide pressure range by use of the collisionally narrowed line profiles. Line parameters measured with TTFMS showed excellent agreement with the parameters measured with direct absorption. The experimental technique used constant-current fast-wavelength scanning, which improved measurement accuracy. © 1997 Optical Society of America

*Key words:* frequency-modulation spectroscopy, high-resolution spectroscopy, diode laser, oxygen.

## 1. Introduction

Diode-laser absorption spectroscopy based on frequency modulation (FM) is a method of choice for gas concentration measurements in which high sensitivity and fast time response are required.<sup>1-6</sup> Although a variety of FM schemes exist, the common underlying concept is a movement of the detection band to a high-frequency region in which the laser source ( $1/f$ ) noise is avoided and signal detection is performed with frequency and phase-sensitive electronics. Depending on the number of modulation tones, the choice of modulation frequency relative to the width of the studied absorption feature, and the detection frequency, the method is referred to as wavelength modulation spectroscopy (WMS),<sup>7</sup> frequency modulation spectroscopy (FMS),<sup>8</sup> or two-tone frequency modulation spectroscopy (TTFMS).<sup>9</sup> In TTFMS the laser is modulated by two closely spaced

frequencies, which are comparable with or larger than the width of the absorbing feature of interest, and the phase-sensitive detection of an absorption-related beat tone is at the intermediate frequency, i.e., the difference frequency, chosen to lie in the low-noise region of the laser. Both FMS and TTFMS, with high-frequency detection, offer the possibility of quantum noise limited detection at a  $10^{-7}$ – $10^{-8}$  fractional absorption.<sup>10-12</sup> In practice, however, optical interference effects in the laser beam path often limit the sensitivity to approximately  $10^{-6}$ . Nevertheless, as we show in our paper, this detection limit allows accurate analysis of line shapes from very weak absorptions.

In quantitative concentration measurements by FM techniques, the line-shape peak-to-peak value is calibrated typically with a reference gas or an absorption spectrum recorded with direct detection. However, accurate measurements under variable linewidth conditions, such as those over a wide range of concentrations, temperatures, and pressures, require information about the line parameters and an adequate theory of the heterodyne-detected signal. Line-shape analysis by least-squares fitting of an assumed line profile to experimental data, yielding accurate line-shape information, was demonstrated only in a few papers with FMS<sup>13</sup> and TTFMS.<sup>14,15</sup> A least-squares fitting procedure, with an appropriate theory of the detected signal and well-known line parameters,

---

When this research was performed, V. G. Avetisov and P. Kauranen were with the Division of Atomic Physics, Lund Institute of Technology, P.O. Box 118, S-221 00 Lund, Sweden. V. G. Avetisov is now with the Norsk Elektro Optikk A/S, Solheimveien 62A, P.O. Box 384, 1471 Skårer, Norway.

Received 11 December 1995; revised manuscript received 16 August 1996.

0003-6935/97/184043-12\$10.00/0

© 1997 Optical Society of America

is used to increase not only the accuracy of quantitative concentration measurements but also the accuracy of measurements of gas parameters such as temperature, velocity, and pressure.<sup>16,17</sup> The ability to perform high-sensitivity measurements with high accuracy in a varying environment is important in areas such as combustion diagnostics and chemical analysis.

Of the various FM techniques, TTFMS seems to be the most suitable for high-accuracy quantitative measurements based on data modeling. The reasons for this are many. The electric-field approach adopted in the theories of FMS and TTFMS is valid at arbitrary modulation frequencies,<sup>18</sup> whereas the intensity approach commonly adopted in WMS theory is limited to low modulation frequencies. In WMS the large modulation index necessary to achieve an optimum signal amplitude generates a multitude of sideband components in the field spectrum, which makes the line-shape calculation in the electric-field approach complicated. In the simpler intensity approach, in which the WMS line-shape information is extracted from the dependence of the signal amplitude on the applied modulation current,<sup>19,20</sup> the entire line shape is not considered, which makes the accuracy of the applied theoretical model and the retrieved line parameters difficult to evaluate. In FMS the absorption and dispersion components in quadrature are of similar amplitude, which requires high accuracy in the adjustment of the detection phase for unambiguous retrieval of the line-shape information. TTFMS, on the other hand, with its low detection frequency, has a nearly negligible dispersion contribution in recorded line shapes, and, in comparison with WMS, the relatively low number of generated sidebands allows accurate theoretical representation of line shapes, which in turn can result in greater retrieval accuracy.

We recently investigated the validity of the TTFMS theory over a wide range of modulation and line parameters, and we modeled numerically generated line shapes with a nonlinear least-squares fitting procedure for the purpose of providing the optimum choice of modulation frequencies and FM indices for accurate line-shape analysis.<sup>15</sup> Also, the weak dispersion component, which appears in the heterodyne-detected signal when the detection phase is adjusted for maximum signal amplitude, was investigated for various experimental situations. Moreover, nonlinear distortion in the modulation response of the diode laser<sup>21</sup> was considered in the theory, which provided a better description of data.

In the present study we extend our previous investigation of TTFMS for high-accuracy quantitative measurements<sup>15</sup> to experimental data recorded over a broad range of pressures. An extensive test of the reliability of the line parameters derived by the least-squares fitting procedure is performed by comparison of the result with line parameters derived from spectra recorded by use of direct absorption. Further, the high resolution and high sensitivity of the experimental technique employed makes a qualitative comparison of the Voigt profile and collisionally nar-

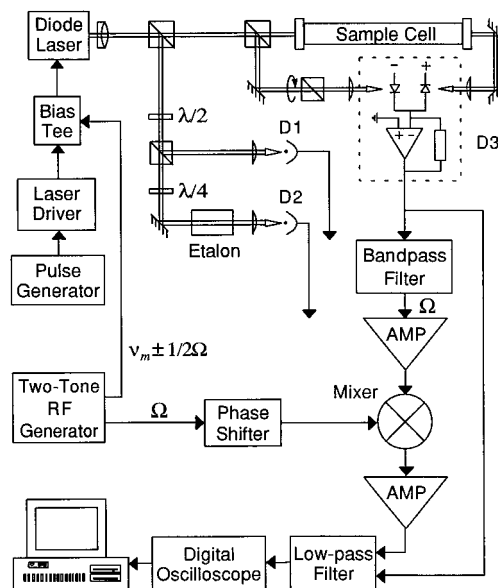


Fig. 1. Schematic of the experimental setup for combined TTFMS and direct absorption measurements.

rowed line profiles possible with both TTFMS and direct absorption.

Experimental techniques for accurate recording of line shapes must exclude effects arising from a variation in the laser spectral characteristics during wavelength scanning. It is known that diode-laser intrinsic properties, such as linewidth, longitudinal mode structure, amplitude and detuning of the relaxation-oscillation sidebands, vary with the laser injection current.<sup>22,23</sup> Also, the modulation characteristics, such as the FM and amplitude modulation (AM) indices and the AM-FM phase difference, depend strongly on the injection current.<sup>23</sup> Thus wavelength scanning of a diode laser by superimposing a saw-tooth current waveform on the laser drive current can produce significant measurement errors. In this study we reduce the effect of injection current variations by superimposing a rectangular waveform on the diode-laser drive current, which produces constant-current wavelength scans.

The experimental arrangement required for recording data with high sensitivity and low instrumental distortion is described. This description includes the constant-current wavelength scanning technique, the data acquisition, and an optical dual-beam subtraction scheme for eliminating background signals and excess laser noise.

## 2. Experimental

Figure 1 shows the basic experimental arrangement. A detailed description of the apparatus is given elsewhere.<sup>3</sup> Here, we describe those parts that are of importance for high-resolution measurements.

### A. Experimental Setup

The diode laser, a double-heterostructure GaAlAs laser manufactured by Mitsubishi (ML4405), operates

in a single mode near 760 nm with a maximum output power of 5 mW. The diverging beam from the laser is collimated by a Newport F-LA40 diode-laser lens and is divided by three cube beam splitters. The first polarizing cube beam splitter passes most of the intensity (70%) to a dual-beam subtraction scheme in which the oxygen cell measurements are made. It passes the rest of the intensity into a side arm with a half-wave ( $\lambda/2$ ) plate and a second polarizing cube beam splitter, which divides the beam and directs it onto two photodetectors, D1 and D2. By rotating the half-wave plate, we can optimize the intensity in either of the two beams after the polarizing beam splitter. At photodetector D1 reference spectra of the oxygen absorption from the ambient air are recorded by use of either direct absorption or TTFMS. The reference spectra are used to determine pressure-induced line shifts and to monitor the laser intensity during the TTFMS cell measurements. At photodetector D2 we obtain a wavenumber scale by recording the intensity transmitted through a solid Fabry-Perot étalon with a free spectral range of  $0.08033 \text{ cm}^{-1}$  and a finesse of 4. The étalon can be replaced by a confocal Fabry-Perot interferometer (FPI) with a free-spectral range of  $0.25 \text{ cm}^{-1}$  (7.5 GHz) and a finesse of approximately 100 for a coarse estimation of the FM index from the sideband-to-carrier intensity ratio and for monitoring the laser output spectral characteristics. The use of a quarter-wave plate ( $\lambda/4$ ) reduces optical feedback into the diode laser from the étalon or the FPI.

The dual-beam subtraction scheme cancels the absorption signal from the ambient oxygen in the beam path outside the absorption cell. The beam is divided by a 50/50 nonpolarizing beam splitter and directed onto two identical photodiodes (photodetector D3), which are mounted on a movable platform for matching the distances travelled by both beams (signal and reference) in open air. The photodiodes, which were carefully selected to have similar transfer characteristics, are connected with opposite polarities to a common transimpedance amplifier. This photodetector configuration maintains background cancellation with high linearity over a broad bandwidth. The passband of the detector was dc to 15 MHz (3 dB), and in this band the subtraction was better than 40 dB. A polarizing cube beam splitter, which deflects part of the reference beam, balances the intensities of the two beams by rotation around the beam axis.

The photodetectors D1, D2, and D3 contain reversed biased p-i-n photodiodes (S-1190 Hamamatsu) and a transimpedance amplifier with a low-noise operational amplifier (Burr-Brown OPA-620).

The stainless steel gas cell, equipped with wedged windows, accommodates an absorption path length of 90 cm. The cell pressure was measured by a CCM Instruments CCM-1000 capacitance manometer, which has a specified accuracy of 0.5% of the reading. Oxygen of 99.998% purity with natural isotope abundance was used in the measurements.

A Melles Griot 06 DLD103 diode-laser driver was

used for current supply and temperature control. The diode laser was biased by a dc current below the threshold. A rectangular current waveform derived from a pulse generator (Tektronix RG501), with current pulses selected with 0.1- to 1-ms duration at repetition rates in the range of 1–0.1 kHz, was superimposed on the laser dc current. The two modulation frequencies ( $\nu_m \pm 1/2 \Omega$ ) were generated by mixing the 585-MHz output of an rf generator (Wavetek 2510A) with the 5.35-MHz output of a sine-wave generator (Tektronix SG 503) in a mixer (Mini-Circuit ZFM-4H). The modulation current passing a variable attenuator was superimposed on the laser drive current by means of a bias tee. The beat signals at  $\Omega = 10.7 \text{ MHz}$  from detectors D1 and D3 were filtered and amplified at 30 dB by a low-noise amplifier (Miteq AU-2A-0110) before demodulation in a double-balanced mixer (Mini-Circuit ZFM-3). A phase shifter with variable delay lines was incorporated for a precise adjustment of the local oscillator phase. The demodulated signals were amplified and low-pass filtered at 1 MHz (Stanford SR560) before data acquisition. The detection bandwidth was carefully selected with respect to the rate at which the laser wavelength is scanned across the absorption lines. When measuring direct transmission, we connected detectors D1 and D3 directly through a low-pass filter (1 MHz) for data acquisition. Great effort was placed on filtering and proper grounding of the electronics.

## B. Data-Acquisition System

The spectra were collected in 1024 channels of data by an 8-bit Tektronix 2431L digital oscilloscope and averaged 1024 times in a personal computer. To enhance the vertical digital resolution of the oscilloscope, we found it necessary to employ different offsets to the incoming waveforms to ensure that the signal was not always digitized by the same portion of the analog-to-digital converter (ADC). During an averaging cycle (for as many as 1024 spectra) the signal offset was moved gradually by the computer software through a total of 16 digitizing levels on the ADC. This way the differential nonlinearity caused by a nonuniform spacing of the digitizing levels in the ADC was effectively reduced.<sup>24</sup> A resolution of better than 12 bits was achieved, which is more than 2 bits better than that obtained by conventional signal averaging. The total nonlinearity, i.e., the general transfer function of the digital oscilloscope, was corrected after a full averaging cycle with a previously measured table of the deviation from an ideal linear transfer function. This procedure improved the linearity of the digital oscilloscope from 0.5% to 0.1% of the full scale of the ADC. The linearity of the complete data-acquisition system, which includes a photodiode, amplifiers, and mixers, was estimated to be better than 0.5% of the maximum scale used.

## C. Wavelength Scanning

A rectangular current pulse with a rise time that was short compared with the growth rate of the junction temperature was used to produce a heat-induced

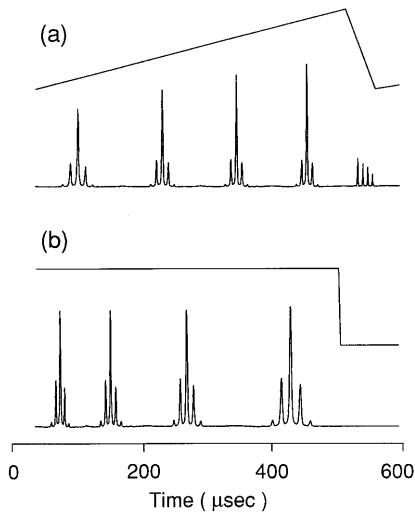


Fig. 2. Comparison of the power spectra of a two-tone frequency modulated laser, which is wavelength scanned with (a) a current ramp and (b) a current pulse. The FM index changes with the laser intensity during the current ramp, whereas a constant FM index is maintained over the wavelength scan induced by the current pulse. The free-spectral range of the Fabry-Perot interferometer was 7.5 GHz.

constant-current wavelength scan under the duration of the pulse.<sup>25,26</sup> There are several advantages to keeping the wavelength-shift-inducing current constant during the wavelength scan. First, variations of the laser intensity and spectral characteristics during the scan are minimized. Second, when direct absorption is used, the zero intensity level can be recorded directly. Third, depending on the pulse duration and repetition rate, the laser can be operated at higher optical powers and temperatures. At the beginning of the current pulse a very high scanning rate in the range of  $0.1\text{--}1\text{ cm}^{-1}/\mu\text{s}$  can be achieved. This has the additional advantage that a single spectrum can be recorded on a short time scale, which reduces the influence of environmental fluctuations. The drawback to a current pulse in comparison with a current ramp is that the induced wavelength shift is more nonlinear. In high-resolution measurement, however, this is not a serious disadvantage because calibration of the relative wave-number scale of the recorded absorption spectra is always required. In our measurements we use recordings of the spectral throughput from a solid Fabry-Perot étalon to linearize the wavelength scale of our spectra computationally.

Figure 2 presents a comparison of the spectral throughput from the FPI, in which an FM laser is wavelength scanned with a current ramp and a rectangular current pulse. A significant change in the sideband-to-carrier ratio (i.e., the FM index) occurs during the current ramp, whereas a nearly constant FM index is maintained during the current pulse. Note that whereas the laser carrier intensity increases linearly with the current ramp, the sideband intensities that depend on the FM current remain constant.

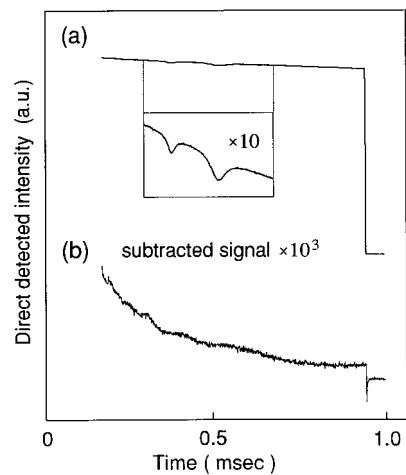


Fig. 3. Demonstration of the efficiency of the dual-beam subtraction scheme. (a) Intensity transmitted through the reference beam showing two atmospheric oxygen lines. The peak absorbance of the stronger line is 1.3%. (b) Signal after subtraction multiplied by  $10^3$ .

Note that heating of the laser-active region during a current pulse slightly raises the threshold current, which in turn causes a small change in the FM index. The relative FM index change during the wavelength scan can be estimated from the change in the laser power. By measuring the FM index from the sideband-to-carrier ratio at different drive currents with an FPI, we observed that the FM index scales with the laser power  $P_0$  approximately as  $1/\sqrt{P_0}$ . Thus a relative FM index change  $\delta\beta$  is related to the relative laser power change  $\delta P_0$  as  $|\delta\beta| \approx 0.5|\delta P_0|$ . In the measurements reported here the threshold current change over a  $2\text{-cm}^{-1}$  single-mode scan produced a 6% change in the laser power, which may result in an FM index change of 3%. For analyzing line shapes with half-widths of approximately  $0.05\text{ cm}^{-1}$ , we note that the corresponding change of the FM index is negligible. If necessary, a highly uniform FM index can be obtained by stabilization of the laser power by electrical feedback or by use of current pulses of a specially designed shape.

#### D. Signal Subtraction by a Dual-beam Configuration

To eliminate the ambient oxygen absorption, we implemented a dual-beam subtraction scheme. Figure 3 demonstrates the performance of the dual-beam subtraction scheme over a  $2\text{-cm}^{-1}$  laser scan with the absorption cell evacuated. The upper trace is the transmitted intensity with one beam blocked, and the lower trace is the recorded signal after subtraction. Both waveforms were accumulated, which yielded an effective detection bandwidth of 2 kHz. The insert shows two magnified atmospheric oxygen lines with the peak absorbance of 1.3%. In the lower trace the detected laser intensity is subtracted to better than  $5 \times 10^{-4}$  over the whole tuning range, and the absorption lines are subtracted to the noise level. The residual slope after subtraction originates from a

wavelength-dependent reflectance of the nonpolarizing cube beam splitter.

The dual-beam subtraction not only cancels the ambient oxygen absorption and the laser intensity but also cancels étalon fringes that originate from multiple reflections in the beam path before the nonpolarizing beam splitter and reduces excess laser noise to below the shot-noise level. By attenuating the laser intensity with neutral-density filters, we verified shot-noise limited detection for both direct absorption and TTFMS. Because shot-noise varies proportionally to the square root of the incident laser power, it can be distinguished from excess laser noise. The measured shot-noise rms value was approximately  $2 \times 10^{-5}$  of the incident laser power in a single scan with a 1-MHz bandwidth. This value coincides with the theoretical value calculated for 2 mW of optical power, accounting for a factor of  $\sqrt{2}$  that is due to the two independent photodiodes.

When the signal-to-noise ratio was being enhanced by signal accumulation, the diode laser was mechanically dithered by a loudspeaker attached to the diode-laser mounting to wash out unwanted étalon fringes. The loudspeaker was driven by a sine wave asynchronously with the wavelength-shifting waveform superimposed on the diode-laser drive current. Vibrating the diode laser is more efficient than vibrating single optical elements or photodetectors<sup>27</sup> because it causes all optical interference in the beam path to be destabilized. Because a spectrum was scanned over a time scale that was short in comparison with the mechanical vibrations, the recorded line shapes were not affected. After signal averaging, étalon fringes limited the detection level to approximately  $2 \times 10^{-6}$  for both TTFMS and direct absorption. In direct absorption, however, the prominent sloping background did not allow this detectivity limit to be practically achieved.

### 3. Measurement Technique

Two oxygen A-band lines, *R15Q16* and *R17R17* centered at 13156.272 and 13156.616  $\text{cm}^{-1}$ , respectively, were selected for use in this investigation. These lines appeared within the continuous tuning range of a laser mode and were recorded simultaneously in one data set. Direct absorption and TTFMS spectra were recorded in two separate measurement series with oxygen pressures ranging from 5 to 400 Torr. As the two oxygen lines are closely spaced, overlapping occurs at high pressures. For better measurement selectivity, the FM index  $\beta$  was chosen to be approximately 0.7, although  $\beta \approx 1$  provides optimum signal amplitude.<sup>15</sup> At three different pressures (30, 200, and 400 Torr) additional spectra were recorded with  $\beta$  changed to approximately 0.5 and 1, respectively. These additional spectra were used to determine the FM index more accurately, as we describe in Subsection 4.C.

Before and after the measurement of each series of absorption spectra, we recorded the spectral throughput of the solid étalon and background spectra with the sample cell evacuated. Because the background was stable throughout the measurements, the back-

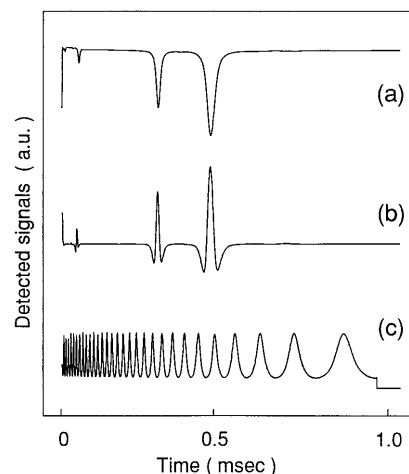


Fig. 4. (a) Direct absorption and (b) TTFMS spectra of oxygen at 200 torr recorded with constant-current wavelength scanning and dual-beam subtraction. (c) Corresponding throughput from the solid étalon.

ground spectra recorded by use of direct absorption and TTFMS were subtracted numerically from the recorded absorption spectra. The recordings of the intensity transmitted through the étalon were used to obtain a relative wave-number scale in the absorption spectra. The reproducibility of the wave-number scale was 0.01% of the  $2\text{-cm}^{-1}$  single-mode scans, which provided sufficient accuracy for the line profile measurements. The accuracy in the relative wave-number scale calibration was determined by the uncertainty of the étalon free-spectral range calibration to approximately 0.05%.

Figures 4(a) and 4(b) show typical spectra of oxygen at 200 Torr recorded with the dual-beam subtraction scheme by use of direct absorption and TTFMS, respectively. Figure 4(c) shows the corresponding étalon spectral throughput. Note the fast wavelength sweep in the beginning of the current pulse. The nonvarying envelopes of the étalon fringes indicate constant laser spectral properties during the wavelength scan.

The pressure dependence of the line-center positions was investigated in a separate measurement sequence with TTFMS. The pressure-induced line shift was measured relative to the line-center position of the ambient oxygen line in a simultaneously recorded TTFMS reference spectrum. Because variations in the ambient pressure controlled by a mercury manometer were less than 0.1% during the measurement sequence, the atmospheric oxygen lines provided a good reference. The peak absorption in the reference beam was 3%. After linearization of the wavelength scale in the recorded spectra, the line-shape peaks were fitted to parabolas and the line shift determined. At the modulation frequencies employed in this study, use of TTFMS for determining line shifts was advantageous because the peak of a recorded line shape was narrower than the peak of the corresponding direct absorption line shape.<sup>15</sup>

#### 4. Data Analysis

##### A. Processing of Spectra

Although a dual-beam subtraction is performed, the ambient oxygen absorption in the air path cannot be disregarded in an accurate line-shape analysis. According to the Beer–Lambert law, the direct absorption signal after subtraction  $I_S(\nu)$  is

$$I_S(\nu) = I_0(\nu)\exp[-\alpha^c(\nu) - \alpha^a(\nu)] - I_0(\nu)\exp[-\alpha^a(\nu)], \quad (1)$$

where  $I_0(\nu)$  is the nonabsorbed transmitted intensity, which is assumed to be equal in both beams, and  $\alpha^c(\nu)$  and  $\alpha^a(\nu)$  are dimensionless absorbances caused by oxygen absorption in the cell and in the air path, respectively. From Eq. (1) the absorbance of the oxygen in the cell is

$$\alpha^c(\nu) = -\ln\{1 + [I_S(\nu)/I_{\text{air}}(\nu)]\}, \quad (2)$$

where

$$I_{\text{air}}(\nu) = I_0(\nu)\exp[-\alpha^a(\nu)] \quad (3)$$

is the intensity transmitted through the open air. The intensity  $I_{\text{air}}(\nu)$  was recorded with the signal beam blocked, and in the subsequent analysis all the direct absorption spectra were processed according to Eq. (2).

For a detailed analysis of TTFMS spectra, appropriate expressions for the heterodyne-detected signal are essential. In previous research<sup>15</sup> we developed the TTFMS theory for accurate line-shape modeling; here, we give only a summary relevant to this study.

When a laser at frequency  $\nu_c$  is modulated by two closely spaced radio frequencies of  $\nu_1 = \nu_m + 1/2\Omega$  and  $\nu_2 = \nu_m - 1/2\Omega$ , the electric field produced is both phase and amplitude modulated. The absorption-related signal, neglecting the dispersion contribution, after phase-sensitive detection of the intensity component at  $\Omega$  is given by

$$I_\Omega = 2I_0 \cos(\theta) \sum_{n,m} \text{Re}(R_{n,m})\exp[-1/2(\alpha_{n,m} + \alpha_{n+1,m-1})], \quad (4)$$

where

$$R_{n,m} = r_n r_m r_{n+1}^* r_{m-1}^* + J_{n+1}(\beta) J_{m-1}(\beta) A_{n,m} + J_n(\beta) J_m(\beta) A_{n+1,m-1}^*, \quad (5)$$

$$r_n(\beta, M, \Psi) \equiv J_n(\beta) + (M/2i)[J_{n-1}(\beta)\exp(i\Psi) - J_{n+1}(\beta)\exp(-i\Psi)]. \quad (6)$$

Here,  $1/2\alpha_{n,m} \equiv 1/2\alpha(\nu_c + n\nu_1 + m\nu_2)$  is the attenuation experienced by the frequency component at  $\nu_c + n\nu_1 + m\nu_2$ ,  $\theta$  is the detection phase angle,  $\beta$  is the FM index,  $M$  is the AM index,  $\Psi$  is the phase difference between AM and FM, and  $A_{n,m}$  is a correction term for a second-order nonlinear distortion of the diode-laser frequency modulation response. In Ref. 15 it was shown that accounting for the nonlinear distortion at the second-harmonic only provides suf-

ficient accuracy for modeling TTFMS line shapes. In this case  $A_{n,m}$  is

$$A_{n,m} \equiv J_m(\beta)\delta_n + J_n(\beta)\delta_m, \quad (7)$$

where

$$\delta_n(\beta, \zeta, \vartheta) \equiv J_1(\zeta)[J_{n-2}(\beta)\exp(i\vartheta) - J_{n+2}(\beta)\exp(-i\vartheta)]. \quad (8)$$

Here  $\zeta$  and  $\vartheta$  are the amplitude and the phase shift, respectively, of the second-harmonic distortion component.

After dual-beam subtraction, the heterodyne-detected signal can be expressed as

$$I_\Omega = 2I_0 \cos(\theta) \sum_{n,m} \text{Re}(R_{n,m})\exp\{-\alpha^a[\nu_c + (n+m)\nu_m]\} \times \{\exp[-1/2(\alpha_{n,m}^c + \alpha_{n+1,m-1}^c)] - 1\}, \quad (9)$$

where it is assumed that two closely spaced sidebands experience the same attenuation from the atmospheric broadened oxygen  $1/2\alpha^a$ , i.e., approximating  $\nu_1 \equiv \nu_2 \equiv \nu_m$ . The recorded TTFMS spectra were normalized to the transmitted nonabsorbed intensity  $I_0(\nu)$ , which was numerically derived from a recording of the intensity  $I_{\text{air}}(\nu)$ . Furthermore, the spectral dependence of  $\exp[\alpha^a(\nu)]$  was derived from the same recording of  $I_{\text{air}}(\nu)$  and used in Eq. (9) to calculate the atmospheric attenuation of  $\alpha^a[\nu_c + (n+m)\nu_m]$  for the different frequency components.

The absorbance  $\alpha(\nu)$  can be expressed in terms of the integrated intensity  $S$  and the line-shape function  $g(\nu - \nu_0)$  as

$$\alpha(\nu) \equiv Sg(\nu - \nu_0). \quad (10)$$

The integrated intensity  $S$  is defined as  $S \equiv S_0PL$ , where  $S_0$  is the line strength,  $P$  is the partial pressure of the absorbing gas, and  $L$  is the absorption path length. In this analysis the line-shape function is described by the Voigt ( $V$ ), Galatry ( $G$ ) soft-collision,<sup>28</sup> or Rautian–Sobelman ( $R$ ) hard-collision<sup>29</sup> profiles. The line profiles are standardized according to Herbert,<sup>30</sup> and the dimensionless line-shape parameters are  $x \equiv (\nu - \nu_0)/\sigma$ ,  $y \equiv \Gamma/\sigma$ , and  $z \equiv \xi/\sigma$ , where  $\nu - \nu_0$  is the frequency deviation from the possibly shifted line center,  $\sigma$  is the Doppler half-width at  $1/e$  intensity,  $\Gamma$  is the collision-induced half-width at half maximum, and  $\xi$  is the narrowing, i.e., the effective velocity-changing collision rate. In this notation the dimensionless absorbance is expressed as

$$\alpha(\nu) \equiv (S/\sigma\sqrt{\pi})K(x, y, z), \quad (11)$$

where  $K(x, y, z)$  is a general standardized line profile function.

A nonlinear least-squares fitting procedure was developed for analyzing direct absorption and TTFMS line shapes with the Voigt, Galatry, or Rautian–Sobelman profiles. The analytical expressions adopted for the line profile functions can be found in Ref. 15 and in references cited therein.

The adjustable line parameters in the least-

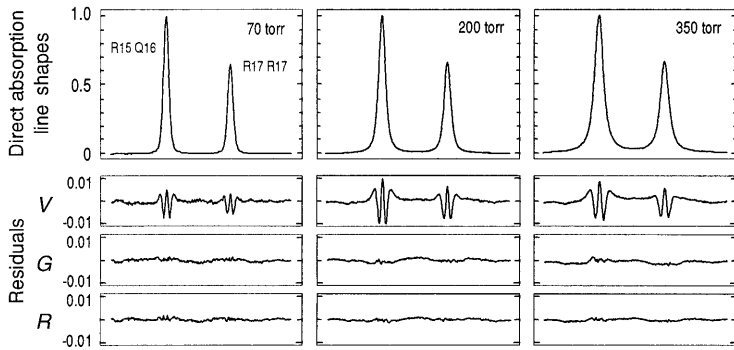


Fig. 5. Typical results of least-squares fits to data recorded by use of direct absorption at three different pressures. The spectra are normalized to their peak amplitudes. The fitted line profiles are the Voigt, Galatry, and Rautian–Sobelman, labeled *V*, *G*, and *R*, respectively.

squares fitting procedure were  $S$ ,  $\nu_0$ ,  $y$ , and  $z$  (denoted equally for  $G$  and  $R$ ). The Doppler half-width was fixed to the theoretical value of  $0.01443 \text{ cm}^{-1}$ , i.e.,  $\sigma = 0.01733 \text{ cm}^{-1}$ . In the fits to the TTFMS line shapes, the AM index  $M$  was an adjustable parameter, the FM index was either adjustable or fixed, and the AM–FM phase difference was fixed to  $\Psi = \pi/2$ , which is a good approximation as demonstrated numerically in Ref. 15. Before the nonlinear least-squares fits of the two oxygen line shapes, the weak absorption features in the recorded spectra from the diode-laser relaxation-oscillation sidebands and oxygen isotopes were removed with a linear fit of a line profile to each of these features. The line profile used in this procedure was obtained from a nonlinear least-squares fit to the R15Q16 line. The removal of the weak spectral features did not influence the line parameter retrieval noticeably; however, it facilitated the evaluation of the residuals of the fits.

Figure 5 shows three direct absorption spectra at different pressures and plots of the residuals from least-squares fits with the Voigt, Galatry, and Rautian–Sobelman profiles. The total oxygen pressures in the cell were 70, 200, and 350 Torr, which yielded the peak absorbances of 2.4%, 4.7%, and 5.9%, respectively. The characteristic deviation of the fitted Voigt profile from the data indicates the effect of collisional (Dicke) narrowing.<sup>31,15</sup> We verified that the nonlinearity of the detection system ( $<0.5\%$ ) and the errors in determining the relative wave-number scale ( $<0.05\%$ ) could not produce a signal distortion with similar appearance and magnitude. Instead, use of the Galatry and Rautian–

Sobelman profiles in the least-squares fitting procedure provided excellent fits to the data.

Figure 6 shows typical results of the least-squares fits of the TTFMS line shapes. The upper traces are the TTFMS spectra at the same pressures used in the direct absorption recordings in Fig. 5, and below are the residuals from fits with the Voigt, Galatry, and Rautian–Sobelman profiles. The FM index  $\beta$  was derived separately, as discussed in Subsection 4.C., and fixed to 0.73. The phase shift of the second-harmonic distortion was set to  $\vartheta = \pi$ ,<sup>32</sup> and the distortion amplitude  $\zeta$  was set to  $\zeta = 0.02\beta$ , which provided the best fit in a fitting sequence in which the distortion amplitude was manually adjusted. Accounting for the second-harmonic distortion in the modeling reduced the residuals by a factor of 3. The characteristic signature in the residuals from the least-squares fits with the Voigt profile are consistent with the residuals obtained from fits to synthetic collisionally narrowed line shapes.<sup>15</sup> Note that these residuals are of the same magnitude as the residuals obtained from the fits to the direct absorption line shapes in Fig. 5. Because the results of the least-squares fits with the collisionally narrowed line profiles are nearly identical, the Rautian–Sobelman profile is used for computational simplicity in the subsequent analysis unless otherwise stated.

#### B. Collisional Narrowing

The narrowing parameter  $\xi$  retrieved from a direct absorption spectrum is influenced by the baseline determination. Especially if the line wings extend over a considerable part of the recorded spectrum, a

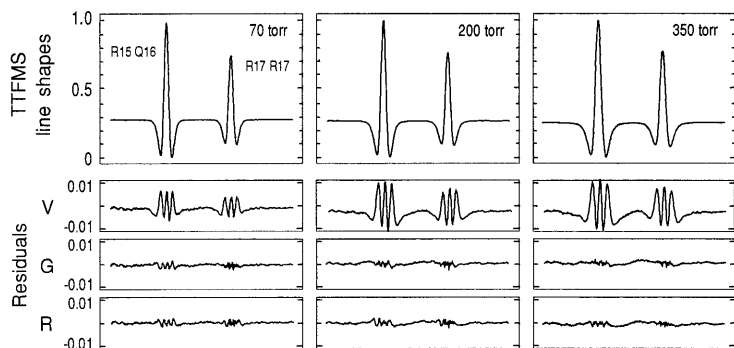


Fig. 6. Typical results of least-squares fits to experimental data recorded by use of TTFMS with measurement conditions corresponding to those in Fig. 5. The modulation indices were  $\beta = 0.73$  and  $M = 0.004$ , and the modulation frequencies were  $585 \pm 5.4 \text{ MHz}$ . Each spectrum is normalized to its peak-to-peak amplitude.

correct baseline determination is difficult. For this reason we performed a separate least-squares fitting sequence with the line parameters adjustable and the modulation parameters fixed to obtain the pressure dependence of the narrowing. In the subsequent data analysis we use the determined narrowing coefficient  $\xi/P$  to calculate the narrowing parameter  $\xi$  at an arbitrary pressure. This procedure improves the retrieval accuracy of the remaining adjustable parameters.

The narrowing coefficient  $\xi/P$  was determined to be  $0.010 \pm 0.001 \text{ cm}^{-1}/\text{atm}$  for the Rautian–Sobelman profile and  $0.013 \pm 0.002 \text{ cm}^{-1}/\text{atm}$  for the Galatry profile. These narrowing coefficients are average values of data obtained from both oxygen lines. Our results are in agreement with the values presented by Ritter and Wilkerson<sup>33</sup> of 0.01 (*R*) and 0.0145  $\text{cm}^{-1}/\text{atm}$  (*G*). (The uncertainties were not given.)

Also in TTFMS, the retrieved narrowing parameter  $\xi$  is influenced by the baseline determination. However, because the TTFMS signal appears from a nearly zero baseline and the spectral extents<sup>15</sup> of the TTFMS line shapes in these measurements were smaller than those for the corresponding direct absorption line shapes, the baseline can be determined more accurately. Accordingly, the narrowing parameters retrieved from TTFMS line shapes showed a more linear and less scattered pressure dependence. The narrowing coefficient  $\xi/P$  was determined to be  $0.0097 \pm 0.0007 \text{ cm}^{-1}/\text{atm}$  (*R*), which agrees with the measurements obtained by use of direct absorption. In the following analysis of both direct absorption and TTFMS line shapes, the value of  $0.01 \text{ cm}^{-1}/\text{atm}$  for the narrowing coefficient  $\xi/P$  is adopted.

### C. FM index Determination

Since the retrieval of the broadening parameter  $\gamma$  and the integrated intensity parameter  $S$  correlates strongly with the FM index  $\beta$ ,<sup>15</sup> an accurate assignment of the FM index parameter  $\beta$  is important. By using a method described in Ref. 14 where at least two spectra are recorded at the same pressure but with different FM indices, we can determine the experimental FM index more accurately. For each spectrum a sequence of least-squares fits is performed with the FM index parameter  $\beta$  differently fixed around the value estimated with an FPI. As a result for each recorded spectrum the line parameters are retrieved as a function of the FM index parameter  $\beta$ . A plot of the derived broadening parameter  $\gamma$  versus the integrated intensity parameter  $S$  shows different slopes for spectra recorded with different experimental FM indices. The plotted traces intersect where the FM indices used in the fittings coincide with their true values. With this method not only is the FM index determined with higher accuracy than it would be from a single fit with an adjustable  $\beta$  or by use of an FPI, but the collision halfwidth  $\Gamma$  and the integrated intensity  $S$  are as well. Figure 7 shows plots of  $\Gamma$  versus  $S$  obtained for the *R15Q16* line at three different pressures for three different experimental FM indices. For comparison,

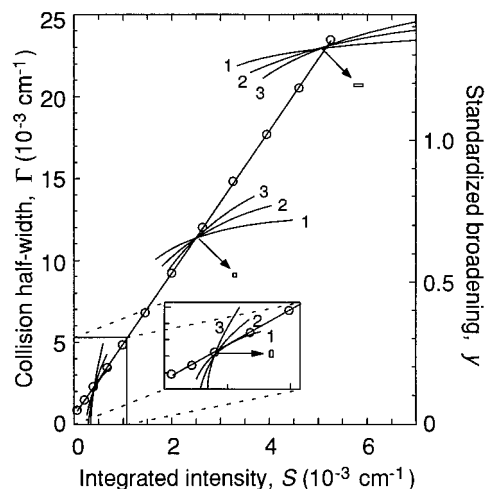


Fig. 7. Collision half-width  $\Gamma$  and standardized broadening  $\gamma$  versus integrated intensity  $S$  for the *R15Q16* line. The traces, labeled 1, 2, and 3, are results of multiple least-squares fits of three TTFMS spectra recorded with different unknown FM indices. The intersection points yield accurate estimations of the collision half-width  $\Gamma$ , the integrated intensity  $S$ , and the FM indices. The rectangles pointed out by arrows indicate the accuracy in determining the line parameters. For comparison, data (open circles) retrieved from direct absorption spectra are shown together with a fitted straight line.

data obtained from the direct absorption spectra (circles) with a fitted straight line are also shown. For a particular pressure the traces are steeper for a larger experimental FM index  $\beta$ , and with increasing pressure the traces become flatter. The agreement between the intersection points and the direct absorption measurements demonstrates the efficiency of the intersection method in deriving accurate line-shape information with TTFMS. The accuracy in the determined collision half-width  $\Gamma$  and the integrated intensity  $S$  can be estimated from the intersection areas. In Fig. 7 the determination errors are indicated by the rectangles. The FM index parameter  $\beta$  increases from the right to the left in the figure: from 0.4 to 0.65 in the flattest traces, from 0.6 to 0.85 in the middle traces, and from 0.8 to 1.05 in the steepest traces. The three experimental FM indices estimated from the intersection points are 0.52, 0.73, and 0.92 with 1% accuracy. Note that the accuracy of the intersection point determination increases with the difference in the experimental FM indices. When the FM index  $\beta$  was adjusted in the least-squares fitting sequence, the average value of  $\beta = 0.72 \pm 2.5\%$  was derived. In the subsequent analysis, the FM index value of 0.73 is adopted.

## 5. Results and Discussion

### A. Line Broadening

The upper part of Fig. 8 shows the collision halfwidth  $\Gamma$  retrieved with direct absorption versus pressure for both oxygen lines. The data for the *R17R17* line was offset by  $0.006 \text{ cm}^{-1}$  for clarity. The broadening coefficients  $\Gamma/P$  were determined from straight line fits to

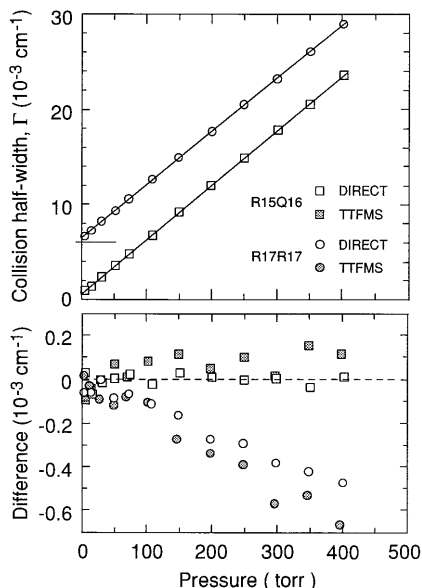


Fig. 8. Collision half-width versus pressure, retrieved from direct absorption and TTFMS line shapes. For clarity the upper plot shows only the direct absorption data with fitted straight lines, and the values for the *R17R17* line are offset. The lower plot shows the difference between the retrieved collision half-widths and the straight line fitted to the retrieved collision half-widths of the *R15Q16* line (open squares).

the retrieved collision half-widths. In the lower part of Fig. 8 collision half-widths obtained with TTFMS are also shown. To make a quantitative comparison possible, we subtracted the straight line fitted to the direct absorption data of the *R15Q16* line from the retrieved collision half-widths. This way the difference in the broadening coefficients for the two lines becomes clearly visible. The agreement between the broadening coefficients obtained with TTFMS and direct absorption is better than 0.5%. The broadening coefficients are presented in Table 1 together with the values obtained by Ritter and Wilkerson,<sup>33</sup> who used a Galatry profile in their data modeling. Our values obtained with a Rautian–Sobelman profile are approximately 3% lower. Use of a Galatry profile in the least-squares fits of the direct absorption line shapes resulted in a 1% increase of the broadening coefficients. The collision half-widths retrieved with the Voigt profile exhibited a nonlinear pressure dependence, owing to the effect of collisional narrowing, with an almost 10% change of the slope in the measured pressure range. A straight line fit to these data provided 3%

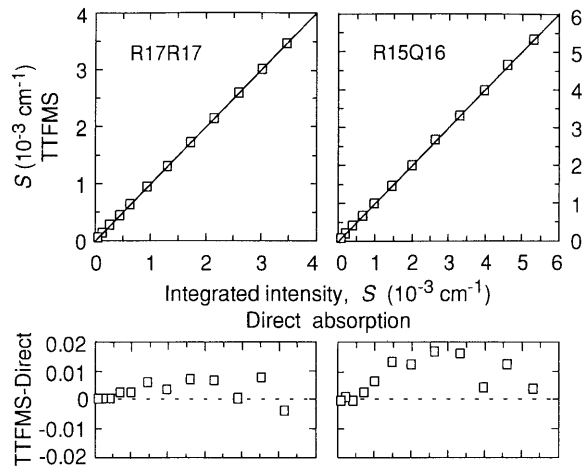


Fig. 9. Integrated intensities retrieved by TTFMS versus integrated intensities retrieved by direct absorption. The lower plot is the difference.

lower values of the broadening coefficients than obtained with the Rautian–Sobelman profile for both the TTFMS and the direct absorption spectra. As a result we conclude that the prominent collisional narrowing of the oxygen *A*-band lines should be considered in an accurate determination of the broadening coefficients.

#### B. Integrated Intensity

The integrated intensities retrieved with TTFMS and direct absorption agree better than 1% in the measured pressure range, as illustrated in Fig. 9, in which the obtained TTFMS data are plotted versus the direct absorption data. The lower part of the figure shows the difference between these data sets. The line strength ( $S_0$ ) determination with TTFMS was possible after calibrating the TTFMS spectrum of the *R17R17* line at 300 torr to the corresponding direct absorption spectrum. The integrated intensity ( $S$ ) values retrieved from the TTFMS and the direct absorption line shapes coincide better than 1% in the measured pressure range, which demonstrates the reliability of TTFMS in measuring the integrated intensity over a wide pressure range. The line strength  $S_0 = S/PL$  of both oxygen transitions was determined from straight line fits to the integrated intensity data. The obtained values, which are presented in Table 1, are between the values presented in Refs. 33 and 34.

In many applications only relative integrated in-

Table 1. Line Parameters Determined in This Study at  $T = 296$  K and Literature Data<sup>a</sup>

A-band Oxygen Line	Self-Broadening Coefficient ( $\text{cm}^{-1}/\text{atm}$ )			Line Strength ( $10^{-24} \text{ cm}^{-1}/\text{mol cm}^{-2}$ )				Self-Shift Coefficient ( $10^{-3} \text{ cm}^{-1}/\text{atm}$ )	
	TTFMS	Direct	Ref. 33	TTFMS	Direct	Ref. 33	Ref. 34	TTFMS	Ref. 35
<i>R15Q16</i>	0.0437 (3)	0.0435 (2)	0.0449 (9)	4.51 (6)	4.50 (3)	4.89 (11)	4.21	-5.75 (10)	-5.5
<i>R17R17</i>	0.0422 (2)	0.0424 (2)	0.0433 (5)	2.93 (4)	2.93 (3)	3.14 (4)	2.74	-6.10 (15)	-5.8

<sup>a</sup>Numbers in parentheses represent statistical error (2 std). Systematic errors are discussed in the text.

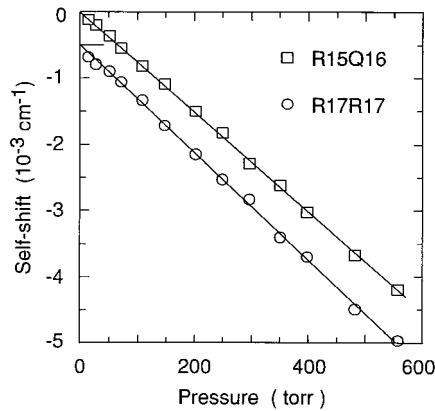


Fig. 10. Self-induced line shifts measured by TTFMS versus pressure. The values for the *R17R17* line are offset for clarity.

tensities are of interest, e.g., in gas temperature determination from the relative intensity ratio of different vibrational-rotational transitions and in concentration measurements calibrated to a reference absorption line. The ratio of the line strengths of the two oxygen lines was determined with the previously derived integrated intensities. The obtained average values were  $1.538 \pm 0.008$  and  $1.536 \pm 0.005$  with TTFMS and direct absorption, respectively. The value provided by the HITRAN database<sup>34</sup> of 1.535 is within our experimental uncertainty.

### C. Self-induced Pressure Shift

Pressure-induced line shifts were measured with TTFMS. Figure 10 shows a plot of the line-center shift as a function of pressure. The data for the *R17R17* line were offset for clarity. From the straight line fits to the measured line shifts of the *R15Q16* and *R17R17*, the self-induced pressure-shift coefficients were determined to be  $-(5.75 \pm 0.10) \times 10^{-3}$  and  $(6.10 \pm 0.15) \times 10^{-3} \text{ cm}^{-1}/\text{atm}$ , respectively. The obtained values are in close agreement with the previous results<sup>35</sup> presented in Table 1.

## 6. Error Analysis

The uncertainties presented in Table 1 are statistical errors. Possible systematic errors are discussed below.

### A. Line Broadening

A very decisive parameter in the least-squares fit of TTFMS line shapes is the FM index  $\beta$  because it correlates with both the broadening  $y$  and the integrated intensity  $S$  parameters. When the TTFMS data were refitted with the FM index  $\beta$  adjustable, it produced approximately six times larger scatter of the retrieved line parameters. The values of the derived broadening coefficients, however, were not affected. This coincides with the results of the numerical modeling in Ref. 15, in which the empirical expression for the absolute broadening error  $dy_\beta$  induced by an error  $d\beta$  of the FM index was derived:

$$dy_\beta \cong -Q_\beta^y(1+y)\beta^{1.5} d\beta, \quad (12)$$

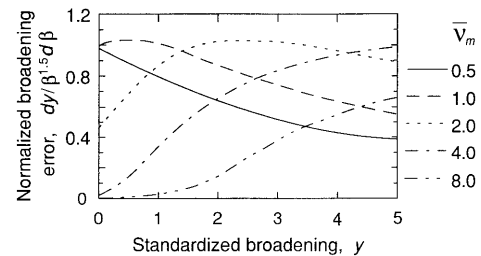


Fig. 11. Error  $dy$  of the broadening parameter induced by an FM index error  $d\beta$  versus the broadening parameter  $y$  for different normalized modulation frequencies  $\bar{\nu}_m$ . In the regions where the error  $dy$  is nearly constant, an FM index error only offsets the pressure dependence of retrieved broadening parameters.

where the coefficient  $Q_\beta^y$  depends on the ratio  $\nu_m/\Delta$  and  $\Delta$  is the absorption line half-width at half maximum. Figure 11 shows plots of the absolute broadening error  $dy_\beta$ , normalized to  $\beta^{1.5} d\beta$ , versus the broadening parameter  $y$  for different values of the normalized modulation frequency  $\bar{\nu}_m = \nu_m/\sigma$ . The data are results of least-squares fits with a Voigt profile to numerically generated TTFMS line shapes. For  $\bar{\nu}_m = 1$ ,  $dy_\beta$  varies little if  $y \leq 1.5$ , which implies that in this region an error in the assignment of the FM index  $\beta$  only offsets the retrieved broadening parameters  $y$  and does not affect the determination of the broadening coefficient  $\Gamma/P$ . Thus with  $\bar{\nu}_m = 1.13$  and  $y$  ranging from 0 to 1.35 (see Fig. 7), an FM index error should induce a negligible systematic error in the determination of the broadening coefficients. This was also verified by refitting the experimental TTFMS line shapes with the incorrectly fixed FM index  $\beta$ .

The differences in phase shifts experienced by different frequency components give rise to a weak intensity component beating at the intermediate frequency  $\Omega$  in quadrature with the absorption component. This dispersion-induced component might contribute significantly in a recorded line shape if the heterodyne-detection phase is not carefully adjusted for the absorption component or if the phase is adjusted for optimum signal amplitude.<sup>15</sup> When determining the collision halfwidth  $\Gamma$ , we find that the dispersion component can cause systematic errors. For this reason the detection phase should be carefully adjusted for the absorption component. In this study, in which the detection phase was adjusted to the absorption component with an accuracy of  $\pm 5^\circ$ , the dispersion component can contribute as much as 0.2% of the recorded line shape.<sup>15</sup> We estimate the introduced uncertainty in the derived collision half-width at 0.2%.

The main systematic errors in determining the self-broadening coefficients originate from the detection nonlinearity of 0.5% and the absolute calibration of the capacitance manometer of 0.5%. There is also a deviation in the results obtained by the different collisional model, e.g., the soft collision model (*G*) provides approximately 1% larger values of the broadening coefficients than the hard collision model (*R*). The adopted value of the narrowing coefficient

$\xi/P$  influences the derived broadening coefficient  $\Gamma/P$  negligibly; e.g., a 10% change in the assignment of narrowing coefficient  $\xi$  leads to a less than 0.3% change in the derived broadening coefficient. Additional systematic errors that are due to the accuracy of the relative wave-number scale and determination of the gas temperature and gas purity are negligible.

Extrapolation of the collision half-widths in Fig. 8 to zero pressure reveals a residual broadening of approximately 20 MHz for both lines, which we attribute to the laser linewidth and the instrumental broadening of the line shape during signal accumulation caused by jitter of the trigger position and current and temperature instabilities. However, this residual broadening does not introduce systematic errors in the broadening coefficient  $\Gamma/P$  when it is determined from the slope of the pressure dependence.

### B. Integrated Intensity

When we refitted the TTFMS line shapes with the FM index  $\beta$  fixed to different values, we found that an FM index assignment error  $d\beta$  induces an integrated intensity error  $dS_\beta$ , which approximately follows the relation  $dS_\beta/S \approx -2d\beta/\beta$ . This is in agreement with the numerically derived relation<sup>15</sup>

$$dS_\beta/S \approx -(2.2 + Q_\beta^S \beta^{1.5})d\beta/\beta, \quad (13)$$

where the coefficient  $Q_\beta^S$  is approximately zero for the ratio of  $\nu_m/\Delta$  experimentally realized in this study. Relation (13) implies that an error  $d\beta$  in the FM index affects the determination of the line strength from the pressure dependence of the integrated intensity parameter  $S$ . Although the accuracy of 1% in the determined FM index should introduce a 2% uncertainty in the derived integrated intensity, the integrated intensities determined with TTFMS and direct absorption show a surprisingly good agreement, better than 1% as mentioned, over the investigated pressure range.

Because the absorption spectra and the laser intensity were recorded with different oscilloscope scales, an uncertainty of 2% owing to the relative calibration of the scales is introduced in the line strengths. The ratio of the resonant main mode to the total laser intensity of  $0.96 \pm 0.02$  was determined by estimating the fraction of intensity in the cavity side modes and the relaxation-oscillation sidebands with the high finesse FPI. The accuracy with which this ratio was determined introduces an approximately 2% uncertainty in the line strengths. Again, the detection nonlinearity (0.5%) and the capacitance manometer measurement accuracy (0.5%) contribute to the line strength errors.

Since the same value of the FM index  $\beta$  was employed in the least-squares fits of both oxygen lines, the 0.1% agreement between the line strength ratios derived with TTFMS and direct absorption confirms that an FM index change during the wavelength scan across the lines was negligible.

## 7. Conclusion

The capability of TTFMS in performing quantitative line-shape measurements was demonstrated by the accurate determination of transition line parameters. The results were compared with the line parameters retrieved with direct absorption. Two closely spaced oxygen A-band lines at 760 nm were modeled over a wide range of oxygen pressures. A dual-beam subtraction scheme eliminated excess laser noise and the atmospheric oxygen absorption in the beam path outside the sample cell. The high sensitivity achieved with both TTFMS and direct absorption permitted an accurate analysis of the recorded line shapes and a meaningful comparison of the results obtained by the two methods. By scanning the diode laser wavelength by use of a waveform with rectangular current pulses, we brought the FM index change over the wavelength scan to a minimum, which significantly reduced distortion of the recorded line shapes. It was observed that a constant laser output power over the wavelength scan indicates a constant FM index. In addition, a constant-current wavelength scan also reduces the influence from variations of intrinsic diode-laser characteristics such as linewidth, amplitude and detuning of the relaxation-oscillation sidebands.

A nonlinear least-squares fitting procedure with a Voigt, Galatry, or Rautian–Sobelman profile was used to analyze line shapes recorded with TTFMS and direct absorption. By using a few spectra recorded with different unknown FM indices, which were multiple fitted with the FM index differently fixed, we accurately determined the experimental FM index. Least-squares fits with the FM index adjustable provided nearly the same FM index values; however, the scatter of the retrieved line parameters increased by approximately six times. This implies that in quantitative gas analysis with high accuracy requirements efforts should be made to determine the FM index carefully.

When employing a Voigt line profile in the least-squares fits of line shapes recorded with both TTFMS and direct absorption, we observed systematic discrepancies that clearly indicate the presence of collisional (Dicke) narrowing. By using a Galatry and a Rautian–Sobelman profile, we significantly reduced these deviations. TTFMS line shapes were fitted over a wide range of pressures, and the obtained residuals were less than 0.3%.

Within the experimental uncertainties, the measurements with TTFMS provided the same values of the integrated intensities and pressure-induced self-broadening, shift, and narrowing coefficients as the direct absorption measurements. The determined line parameters were consistent with literature values. The line strength ratio of the two oxygen lines was measured accurately, which is advantageous, for example, for temperature measurements.

In this study TTFMS line shapes from absorbances of a few percent were recorded and treated with such accuracy that even the small effect of collisional narrowing can be quantified. The combination of high

sensitivity and possibility of extracting detailed line-shape information makes TTFMS a useful tool for accurate quantitative gas measurements in a broad area of applications, in particular where direct absorption methods are not feasible.

We are pleased to acknowledge Sune Svanberg for support and valuable suggestions on the manuscript. This research was funded by the Swedish Research Council for Engineering Science and the Swedish Board for Industrial and Technical Development.

## References

1. J. C. Bloch, R. W. Fied, G. H. Hall, and T. J. Sears, "Time-resolved frequency modulation spectroscopy of photochemical transients," *J. Chem. Phys.* **101**, 1717–1720 (1994).
2. D. S. Baer, R. K. Hanson, M. E. Newfield, and N. K. J. M. Gopaul, "Multiplexed diode-laser sensor system for simultaneous H<sub>2</sub>O, O<sub>2</sub>, and temperature measurements," *Opt. Lett.* **19**, 1900–1902 (1994).
3. P. Kauranen, I. Harwigsson, and B. Jönsson, "Relative vapor pressure measurements using a frequency-modulated tunable diode laser, a tool for water activity determination in solutions," *J. Phys. Chem.* **98**, 1411–1415 (1994).
4. P. Kauranen, H. M. Hertz, and S. Svanberg, "Tomographic imaging of fluid flows by the use of two-tone frequency-modulation spectroscopy," *Opt. Lett.* **19**, 1498–1500 (1994).
5. D. A. Glenar, D. E. Jennings, and S. Nadler, "Electrooptic modulation methods for high sensitivity tunable diode laser spectroscopy," *Appl. Opt.* **29**, 2282–2288 (1990).
6. H. Riris, C. B. Carlisle, L. W. Carr, D. E. Cooper, R. U. Martinelli, and R. J. Menna, "Design of an open path near-infrared diode laser sensor: application to oxygen, water, and carbon dioxide vapor detection," *Appl. Opt.* **33**, 7059–7066 (1994).
7. E. G. Moses and C. L. Tang, "High-sensitivity laser wavelength-modulation spectroscopy," *Opt. Lett.* **1**, 115–117 (1977).
8. G. C. Bjorklund, "Frequency-modulation spectroscopy: a new method for measuring weak absorptions and dispersions," *Opt. Lett.* **5**, 15–17 (1980).
9. G. R. Janik, C. B. Carlisle, and T. F. Gallagher, "Two-tone frequency-modulation spectroscopy," *J. Opt. Soc. Am. B* **3**, 1070–1074 (1986).
10. J. A. Silver, "Frequency-modulation spectroscopy for trace species detection: theory and comparison among experimental methods," *Appl. Opt.* **31**, 707–717 (1992).
11. P. Werle, F. Slemr, M. Gehrtz, and C. Bräuchle, "Quantum-limited FM spectroscopy with a lead-salt diode laser," *Appl. Phys. B* **49**, 99–108 (1989).
12. C. B. Carlisle, D. E. Cooper, and H. Preier, "Quantum noise-limited FM spectroscopy with a lead-salt diode laser," *Appl. Opt.* **28**, 2567–2576 (1989).
13. N. C. Wong and J. L. Hall, "High-resolution measurement of water-vapor overtone absorption in the visible by frequency-modulation spectroscopy," *J. Opt. Soc. Am. B* **6**, 2300–2308 (1989).
14. P. Kauranen and V. G. Avetisov, "Determination of absorption line parameters using two-tone frequency-modulation spectroscopy with diode lasers," *Opt. Commun.* **106**, 213–217 (1994).
15. V. G. Avetisov and P. Kauranen, "Two-tone frequency-modulation spectroscopy for quantitative measurements of gaseous species: theoretical, numerical, and experimental investigation of line shapes," *Appl. Opt.* **35**, 4705–4723 (1996).
16. M. P. Arroyo, S. Langlois, and R. K. Hanson, "Diode-laser absorption technique for simultaneous measurements of multiple gasdynamic parameters in high-speed flows containing water vapor," *Appl. Opt.* **33**, 3296–3307 (1994).
17. L. C. Philippe and R. K. Hanson, "Laser diode wavelength-modulation spectroscopy for simultaneous measurement of temperature, pressure, and velocity in shock-heated oxygen flows," *Appl. Opt.* **32**, 6090–6103 (1993).
18. J. M. Supplee, E. A. Whittaker, and W. Lenth, "Theoretical description of frequency modulation and wavelength modulation spectroscopy," *Appl. Opt.* **33**, 6294–6302 (1994).
19. J. Reid and D. Labrie, "Second-harmonic detection with tunable diode lasers: comparison of experiment and theory," *Appl. Phys. B* **26**, 203–210 (1981).
20. N. Goldstein, S. Adler-Golden, J. Lee, and F. Bien, "Measurement of molecular concentrations and line parameters using line-locked second harmonic spectroscopy with an AlGaAs diode laser," *Appl. Opt.* **31**, 3409–3415 (1992).
21. K. Y. Lau and A. Yariv, "Intermodulation distortion in a directly modulated semiconductor injection laser," *Appl. Phys. Lett.* **45**, 1034–1036 (1984).
22. G. P. Agrawal and N. K. Dutta, *Long-wavelength Semiconductor Lasers* (Van Nostrand Reinhold, New York, 1986).
23. S. Kobayashi, Y. Yamamoto, M. Ito, and T. Kimura, "Direct frequency modulation in GaAlAs semiconductor lasers," *IEEE J. Quantum Electron.* **QE-18**, 582–595 (1982).
24. V. G. Avetisov and P. Kauranen, "A software method for improving the performance characteristics of a conventional digitizing oscilloscope," *Lund Reports on Atom. Phys.* **158** (1994).
25. Y. V. Kosichkin, A. I. Nadezhdinskii, and E. V. Stepanov, "Diode laser spectroscopy of collisional broadening in the spectra of polyatomic molecules," *J. Quant. Spectrosc. Radiat. Transfer* **43**, 499–509 (1990).
26. V. G. Avetisov, A. I. Nadezhdinskii, A. N. Khusnutdinov, P. M. Omarova, and M. V. Zyrianov, "Diode laser spectroscopy of water vapor in 1.8  $\mu\text{m}$ : line profile measurements," *J. Mol. Spectrosc.* **160**, 326–334 (1993).
27. D. S. Bomse, A. C. Stanton, and J. A. Silver, "Frequency modulation and wavelength modulation spectroscopies: comparison of experimental methods using a lead-salt diode laser," *Appl. Opt.* **31**, 718–731 (1992).
28. L. Galatry, "Simultaneous effect of Doppler and foreign gas broadening on spectral shapes," *Phys. Rev.* **122**, 1218–1223 (1961).
29. S. G. Rautian and I. I. Sobelman, "Effect of collisions on the Doppler broadening of spectral lines," *Sov. Phys. Usp.* **9**, 701–716 (1967).
30. F. Herbert, "Spectrum line profiles: a generalized Voigt function including collisional narrowing," *J. Quant. Spectrosc. Radiat. Transfer* **14**, 943–951 (1974).
31. P. L. Varghese and R. K. Hanson, "Collisional narrowing effects on spectral line shapes measured at high resolution," *Appl. Opt.* **23**, 2376–2385 (1984).
32. G. Morthier, F. Libbrecht, K. David, P. Vankwikelberge, and R. G. Baets, "Theoretical investigation of the second-order harmonic distortion in the AM response of 1.55  $\mu\text{m}$  F-P and DFB lasers," *IEEE J. Quantum Electron.* **27**, 1990–2002 (1991).
33. K. J. Ritter and T. D. Wilkerson, "High-resolution spectroscopy of the oxygen A band," *J. Mol. Spectrosc.* **121**, 1–19 (1987).
34. L. S. Rothman, R. R. Gamache, R. H. Tipping, C. P. Rinsland, M. A. H. Smith, D. C. Benner, V. M. Devi, J.-M. Flaud, C. Camy-Peyret, A. Perrin, A. Goldman, S. T. Massie, L. R. Brown, and R. A. Toth, "The HITRAN molecular database: editions of 1991 and 1992," *J. Quant. Spectrosc. Radiat. Transfer* **48**, 469–507 (1992).
35. K. J. Ritter, "A high resolution spectroscopic study of absorption line profiles in the A-band of molecular oxygen," Ph.D. dissertation (University of Maryland, College Park, Md., 1986).